LHCb-CONF-2011-006
May 24, 2011

Tagged time-dependent angular analysis of $B_s^0 \to J/\psi\,\phi$ decays with the 2010 LHCb data

The LHCb Collaboration[1]

Abstract

The interference between B_s^0 decays to $J/\psi\,\phi$ either directly or via B_s^0–$\overline{B}_s^0$ oscillation gives rise to a CP violating phase $\phi_s^{J/\psi\,\phi}$. In the Standard Model, this phase is approximately $-2\beta_s$, where $\beta_s = \arg\left(-V_{ts}V_{tb}^*/V_{cs}V_{cb}^*\right)$. We have performed a measurement of $\phi_s^{J/\psi\,\phi}$ using a sample that contains 836 ± 60 $B_s^0 \to J/\psi\phi$ events extracted from $36\,\text{pb}^{-1}$ of pp collisions collected during the 2010 LHC run at $\sqrt{s} = 7\,\text{TeV}$. The result is presented as a two-dimensional region in the $\phi_s - \Delta\Gamma_s$ plane. The probability of a fluctuation from the Standard Model expectation to the observed result for ϕ_s and $\Delta\Gamma_s$ is 22% ("1.2σ"). We derive a one-dimensional interval at 68% CL of $\phi_s \in [-2.7, -0.5]\,\text{rad}$.

[1]Conference report prepared for *Beauty*, Amsterdam, 4–11 April 2011; contact authors: Wouter Hulsbergen and Olivier Leroy

Contents

1 Introduction

Decays of neutral B mesons provide a unique laboratory to study CP-violation originating from a non-trivial complex phase in the CKM matrix. The relative phase between the *direct* decay amplitude and the amplitude of *decay via mixing* gives rise to time-dependent CP-violation, a difference in the proper decay time distribution of B-meson and anti-B meson decays. The decay $B_s^0 \to J/\psi\phi$ is considered the golden mode for measuring this type of CP violation in the B_s^0 system. In the Standard Model the CP-violating phase in this decay is predicted to be $\phi_s \simeq -2\beta_s$, where $\beta_s = \arg\left(-V_{ts}V_{tb}^*/V_{cs}V_{cb}^*\right)$. The indirect determination via global fits to experimental data gives $2\beta_s = (0.0363 \pm 0.0017)\,\text{rad}$ [1].

Measurements on B^0 decays performed by the B factories severely constrain any beyond the Standard Model contributions to decays via tree topologies or in $B^0 - \bar{B}^0$ mixing. However, new contributions to $B_s^0 - \bar{B}_s^0$ mixing [2, 3] are much less constrained and may alter the expected value of ϕ_s [4, 5]. Previous constraints on ϕ_s in $B_s^0 \to J/\psi\phi$ decays have been reported by the Tevatron experiments CDF [6] and DØ [7], using approximately 6 500 and 3 400 $B_s^0 \to J/\psi\phi$ candidates, respectively. For both experiments the uncertainty on ϕ_s is about 0.5 rad. The precise determination of ϕ_s in $B_s^0 \to J/\psi\phi$ decays is one of the key goals of the LHCb experiment [8].

The LHCb detector is a forward spectrometer at the Large Hadron Collider (LHC) at CERN [9]. In this document we report on the first measurement of ϕ_s in LHCb using a sample that contains 836 ± 60 $B_s^0 \to J/\psi\phi$ decays, extracted from $36\,\text{pb}^{-1}$ of pp collisions collected during the 2010 LHC run at $\sqrt{s} = 7\,\text{TeV}$. The analysis relies on results presented in previous conference reports. In [10] we present the selection and the lifetime measurement of $B_s^0 \to J/\psi(\mu^+\mu^-)\phi(K^+K^-)$ and other $B \to J/\psi X$ channels and demonstrate that it is in agreement with the world average. Understanding the decay time resolution and acceptance is an important ingredient to both the lifetime measurement and the measurement of ϕ_s. The calibration of the flavour tagging using $B^0 \to D^{*-}\mu^+\nu_\mu$, $B^0 \to J/\psi K^{*0}$ and $B^+ \to J/\psi K^+$ decays is reported in [12]. The flavour tagging is applied in a measurement of time-dependent CP-violation in $B^0 \to J/\psi K_S^0$ decays, reported in [13].

The flavour tagging is also used for the analysis of neutral B_s^0 mixing in $B_s^0 \to D_s\pi$ and $B^0 \to D\pi$ decays, respectively reported in [14] and [15]. The measurement of Δm_s in $B_s^0 \to D_s\pi$ demonstrates that the achieved decay time resolution is sufficient to resolve the fast oscillations in B_s^0 mixing. Furthermore, even with the limited statistics of the 2010 run, the Δm_s measurement is already fully competitive with Tevatron measurements. In the future the mixing amplitude in $B_s^0 \to D_s\pi$ is also the main calibration mode for the same-side kaon tagger. However, the current data sample is too small to calibrate this tagger reliably. Therefore, it has not yet been used for the ϕ_s analysis presented here.

Finally, in [11] we report on the untagged angular analysis of $B^0 \to J/\psi K^{*0}$ and $B_s^0 \to J/\psi\phi$ decays. This analysis gives access to the decay amplitudes for both final states, as well as the lifetime and $\Delta\Gamma_s$ for $B_s^0 \to J/\psi\phi$. Due to the forward geometry of the LHCb detector, the reconstruction efficiency for these decays is a non-trivial function of the decay angles. Understanding the acceptance is an important ingredient to these measurements and the measurement of ϕ_s.

The analysis presented here is essentially an extension of the analysis in [11] with flavour tagging information. We do not repeat the details of that analysis here, but instead focus on aspects that have not been previously discussed. The different steps of the analysis are described in Section 2 and the results reported in Section 3.

2 Description of the analysis

The phase ϕ_s is extracted from the data with an unbinned maximum likelihood fit to the candidate invariant mass m, the proper decay time t and the 4-body decay angles in the transversity frame $\Omega = \{\cos\theta, \varphi, \cos\psi\}$, defined in Fig. 1. The selected event sample is dominated by a large background with several distinct contributions:

- random combinations of four prompt tracks;
- background from prompt J/ψ events, combined with two random tracks;
- background due to J/ψ from non-signal $B \to J/\psi X$ decays;
- long lived combinatorial background where the two reconstructed muons do not originate from a true J/ψ decay.

In order to reduce the sensitivity to the description of the prompt contribution, the fit is performed only to events with decay time $t > 0.3$ ps. This reduces the signal yield from 836 ± 60 to 757 ± 28 candidates, but affects the sensitivity to ϕ_s only marginally. The background of signal-like events in the remaining sample is only of the order of a few percent.

The implementation of the likelihood fit has been described in detail in [11], in which we present the so-called *untagged* angular analysis of $B_s^0 \to J/\psi\,\phi$ decays. In this note, there are two main modifications with respect to the fit done in [11]. First, in order to measure time-dependent CP violation and constrain ϕ_s, information on the flavour of the B_s^0 candidate at production is added. The flavour tag takes the form of a discrete flag d, which is $+1$ (-1) for B_s^0 $(\overline{B}_s^0)$, and an estimated per-event mistag probability ω. Including the flavour tag information introduces systematic uncertainties due to imperfect knowledge of the flavour tag dilution, which must be calibrated on control samples. Furthermore, since the asymmetry is modulated by the inverse of the B_s^0–$\overline{B}_s^0$ mixing frequency, which (in contrast to the lifetime) is of the same order as the decay time resolution, uncertainties in the resolution model are now important as well.

Second, in order to exploit the 2010 dataset maximally, events selected by the displaced track trigger (called "lifetime-biased events") are included in the analysis. This increases the number of candidates with decay time $t > 0.3\,\text{ps}$ by about 30%, but requires a modeling of the non-trivial decay time acceptance in the fit.

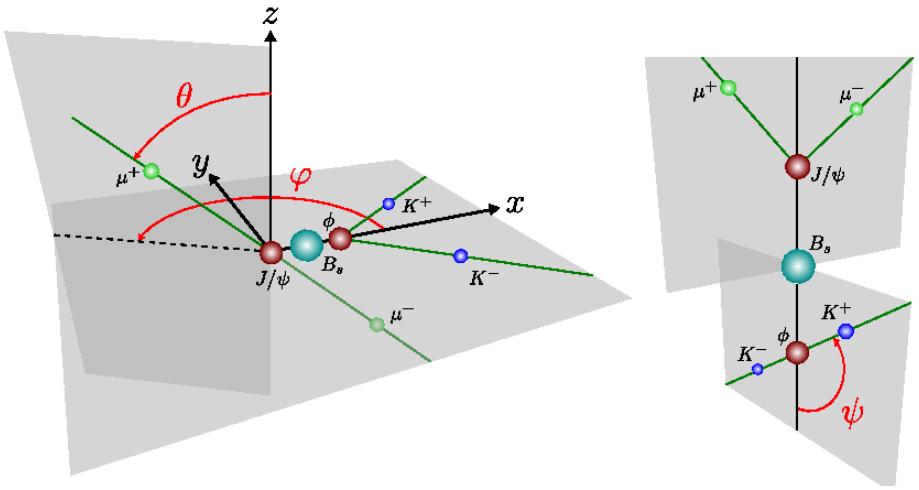

Figure 1: Definition of the decay angles in the transversity frame: θ is the angle formed by the positive lepton (ℓ^+) and the z axis, in the J/ψ rest frame. The angle φ is the azimuthal angle of ℓ^+ in the same frame. In the ϕ meson rest frame, ψ is the angle between $\vec{p}(K^+)$ and $-\vec{p}(J/\psi)$.

2.1 The signal PDF

The likelihood function for N events can be written generically as

$$\mathcal{L} \;=\; \prod_{e}^{N} \mathcal{P}\left(\{m,t,\Omega,d,\omega\}_e;\lambda_{\rm phys},\lambda_{\rm det},\lambda_{\rm bkg}\right)\,, \tag{1}$$

where the probability density function (PDF) $\mathcal{P}$ consists of a signal component $\mathcal{S}$ and a background component $\mathcal{B}$,

$$\mathcal{P} = \; f_{\rm sig}\,\mathcal{S} \;+\; (1-f_{\rm sig})\,\mathcal{B}\,. \tag{2}$$

with $f_{\rm sig}$ the signal fraction. The set of physics parameters $\lambda_{\rm phys}$ includes the B_s^0 decay width Γ_s, the decay width difference between the B_s^0 mass eigenstates $\Delta\Gamma_s$, the mixing frequency Δm_s, the CP violating phase ϕ_s and the relative phases and magnitudes of the three angular transversity amplitudes. The symbol $\lambda_{\rm det}$ represents the parameters involved in describing resolutions, acceptance and flavour tag calibration. The parameters used to describe the background are generically denoted by $\lambda_{\rm bkg}$.

We have verified that the candidate mass does not correlate with the other observables such that the PDF can be factorized. The mass PDFs were described in the untagged analysis [11]. We assume that the shape of the background does not depend on the flavour tag and that it factorizes in decay time and decay angles. The background PDF then reduces to that described in the untagged analysis. Consequently, we concentrate in the following on the PDF for the decay time and decay angles for the signal contribution.

Ignoring detector effects, the distribution for the decay time t and the transversity angles Ω for $B_s^0 \to J/\psi\,\phi$ decays produced in a B_s^0 flavour eigenstate is given by the differential decay rate

$$\frac{\mathrm{d}^4\Gamma(B_s^0 \to J/\psi\phi)}{\mathrm{d}t\;\mathrm{d}\cos\theta\;\mathrm{d}\varphi\;\mathrm{d}\cos\psi} \equiv \frac{\mathrm{d}^4\Gamma}{\mathrm{d}t\;\mathrm{d}\Omega} \propto \sum_{k=1}^{6} h_k(t) f_k(\Omega)\,. \tag{3}$$

The six time-dependent amplitudes $h_k(t)$ and the angular functions $f_k(\Omega)$ are given in Table 1. Expressed in terms of the size $|A_i(0)|$ and phase δ_i of the transversity amplitudes

k	$h_k(t)$	$f_k(\theta,\psi,\varphi)$
1	$\lvert A_0(t)\rvert^2$	$2\cos^2\psi(1-\sin^2\theta\cos^2\varphi)$
2	$\lvert A_{\|\|}(t)\rvert^2$	$\sin^2\psi(1-\sin^2\theta\sin^2\varphi)$
3	$\lvert A_\perp(t)\rvert^2$	$\sin^2\psi\sin^2\theta$
4	$\Im\{A_{\|\|}^*(t)A_\perp(t)\}$	$-\sin^2\psi\sin 2\theta\sin\varphi$
5	$\Re\{A_0^*(t)A_{\|\|}(t)\}$	$\frac{1}{\sqrt{2}}\sin 2\psi\sin^2\theta\sin 2\varphi$
6	$\Im\{A_0^*(t)A_\perp(t)\}$	$\frac{1}{\sqrt{2}}\sin 2\psi\sin 2\theta\cos\varphi$

Table 1: Definition of the functions $h_k(t)$ and $f_k(\theta,\psi,\varphi)$ of Eq. 3

.

at $t=0$, the time dependent amplitudes are given by

$$|A_0(t)|^2 = |A_0(0)|^2 \mathrm{e}^{-\Gamma_s t}\left[\cosh\left(\frac{\Delta\Gamma_s t}{2}\right) - \cos\phi_s \sinh\left(\frac{\Delta\Gamma_s t}{2}\right) + \sin\phi_s \sin(\Delta m_s t)\right], \tag{4}$$

$$|A_{\|}(t)|^2 = |A_{\|}(0)|^2 \mathrm{e}^{-\Gamma_s t}\left[\cosh\left(\frac{\Delta\Gamma_s t}{2}\right) - \cos\phi_s \sinh\left(\frac{\Delta\Gamma_s t}{2}\right) + \sin\phi_s \sin(\Delta m_s t)\right], \tag{5}$$

$$|A_\perp(t)|^2 = |A_\perp(0)|^2 \mathrm{e}^{-\Gamma_s t}\left[\cosh\left(\frac{\Delta\Gamma_s t}{2}\right) + \cos\phi_s \sinh\left(\frac{\Delta\Gamma_s t}{2}\right) - \sin\phi_s \sin(\Delta m_s t)\right], \tag{6}$$

$$\begin{aligned}\Im\{A_{\|}^*(t)A_\perp(t)\} = {} & |A_{\|}(0)||A_\perp(0)|\mathrm{e}^{-\Gamma_s t}\Big[-\cos(\delta_\perp-\delta_{\|})\sin\phi_s\sinh\left(\frac{\Delta\Gamma_s t}{2}\right) \\ & + \sin(\delta_\perp-\delta_{\|})\cos(\Delta m_s t) - \cos(\delta_\perp-\delta_{\|})\cos\phi_s\sin(\Delta m_s t)\Big],\end{aligned} \tag{7}$$

$$\begin{aligned}\Re\{A_0^*(t)A_{\|}(t)\} = {} & |A_0(0)||A_{\|}(0)|\mathrm{e}^{-\Gamma_s t}\cos\delta_{\|}\Big[\cosh\left(\frac{\Delta\Gamma_s t}{2}\right) - \cos\phi_s\sinh\left(\frac{\Delta\Gamma_s t}{2}\right) \\ & + \sin\phi_s\sin(\Delta m_s t)\Big],\end{aligned} \tag{8}$$

$$\begin{aligned}\Im\{A_0^*(t)A_\perp(t)\} = {} & |A_0(0)||A_\perp(0)|\mathrm{e}^{-\Gamma_s t}\Big[-\cos\delta_\perp\sin\phi_s\sinh\left(\frac{\Delta\Gamma_s t}{2}\right) \\ & + \sin\delta_\perp\cos(\Delta m_s t) - \cos\delta_\perp\cos\phi_s\sin(\Delta m_s t)\Big].\end{aligned} \tag{9}$$

where we have chosen a phase convention such that $\delta_0 = 0$. The expressions for the time-evolution for $B_s^0 \to J/\psi\,\phi$ decays produced in a $\overline{B}_s^0$ flavour eigenstate can be obtained from those above by inserting a factor -1 in front of the terms involving mixing ($\sin(\Delta m_s t)$

and $\cos(\Delta m_s t)$). The decay rates are invariant under the simultaneous transformation

$$\begin{array}{rcl} \phi_s & \longleftrightarrow & \pi - \phi_s \\ \Delta\Gamma_s & \longleftrightarrow & -\Delta\Gamma_s \\ \delta_\parallel & \longleftrightarrow & -\delta_\parallel \\ \delta_\perp & \longleftrightarrow & \pi - \delta_\perp \,. \end{array} \tag{10}$$

It may be possible to resolve this two-fold ambiguity by exploiting the interference with an S-wave contribution as discussed in [16]. In our current fit we ignore the S-wave contribution and estimate the corresponding systematic uncertainty on ϕ_s using the upper limit on the S-wave contribution measured by CDF [6].

2.2 Flavour tagging

The signal distributions are corrected for resolution and acceptance effects for both decay time and decay angles and for the dilution from flavour tagging. For the latter, we first divide the PDF into tagged and untagged events. The PDF for the untagged events is identical to the PDF used for the untagged analysis. The PDF for the tagged events is obtained from the distributions in Equation 3 by inserting experimental dilutions in front of the terms involving the mixing in the functions in Equations 4 to 9:

$$\begin{array}{rcl} \sin(\Delta m_s t) & \longrightarrow & d\,\mathcal{D}\,\sin(\Delta m_s t)\,, \\ \cos(\Delta m_s t) & \longrightarrow & d\,\mathcal{D}\,\cos(\Delta m_s t)\,, \end{array}$$

where d is the initial flavour tag decision ($+1$ for B_s^0 and -1 for $\overline{B}_s^0$). The dilution is given by $\mathcal{D} \;=\; 1 - 2\omega$, where ω is the mistag probability.

The optimization and calibration of the flavour tagging is described in [12]. In this analysis we use the per-event mistag probability, exploiting only the "opposite-side" (OS) flavour tagger. The OS flavour tagger uses four different signatures, namely high p_T muons, electrons and kaons, and the net charge of an inclusively reconstructed secondary vertex. Each of these signatures is optimized separately using in a first stage simulated events, and in a second stage the $B^0 \to D^{*-}\mu^+\nu_\mu$ signal in the 2010 data. The decisions of the four taggers are individually calibrated using $B^+ \to J/\psi\, K^+$ decays and combined as explained in [12]. The combination procedure provides an estimated per-event mistag probability. It is again calibrated using $B^+ \to J/\psi\, K^+$ decays assuming a linear dependence between the estimated mistag probability η and the actual mistag probability ω,

$$\omega \;=\; p_0 \;+\; p_1\,(\eta - \langle\eta\rangle)\,, \tag{11}$$

where p_0 and p_1 are calibration parameters and $\langle\eta\rangle$ is the average estimated mistag probability in the calibration sample. (This parameterization is chosen such that the correlation between p_0 and p_1 approximately vanishes.) Their values and correlations $\rho(p_0, p_1)$ extracted from the $B^+ \to J/\psi\, K^+$ sample are given in Table 2. Note that it is no coincidence that p_0 and p_1 are very close to their expected values ($\langle\eta\rangle$ and 1 respectively), since the same sample was used to calibrate the expected mistag. However, the uncertainty on

p_0	p_1	$\langle\eta\rangle$	$\rho(p_0, p_1)$
$0.338 \pm 0.012 \pm 0.004$	$1.01 \pm 0.12 \pm 0.01$	0.339	-0.05

Table 2: Calibration parameters, average mistag and correlations between the calibrations parameters, extracted from the $B^+ \to J/\psi K^+$ control channel [12]. The first error is statistical and the second systematic.

the parameters p_0 and p_1 can be used to propagate the statistical uncertainty on the tagging calibration from the $B^+ \to J/\psi\, K^+$ calibration sample to the result of the fit on the $B_s^0 \to J/\psi\, \phi$ sample.

From the uncertainties on the calibration parameters the effective dilution of the $B_s^0 \to J/\psi\phi$ sample is estimated as

$$\left\langle \mathcal{D}^{\rm tag} \right\rangle_{\rm eff} \;=\; 0.35 \;\pm\; 0.03\,. \tag{12}$$

With an efficiency to obtain a tagging decision of $\varepsilon_{\rm tag} = (17.6 \pm 1.4)\%$, the effective tagging efficiency is $\varepsilon_{\rm tag}\mathcal{D}^2 = (2.2 \pm 0.4)\%$.

The uncertainty in the dilution is dominated by the number of events in the calibration channel. It is included in the confidence intervals presented in the next section by allowing the tagging calibration parameters to vary in the maximum likelihood fit within their known uncertainties.[2] The uncertainty on the mixing frequency is also included in the fit, by varying Δm_s constrained to the CDF measurement of $17.77 \pm 0.12\,{\rm ps}^{-1}$ [17].

With the formalism above we ignore a possible difference of mistag probability between B_s^0 and $\overline{B}_s^0$. Monte Carlo studies indicates a maximum relative difference of $(3.2 \pm 1.7)\%$ [12]. Conservative toy Monte Carlo have been performed with 2.5 times this difference and we observe negligible bias on the measurement of ϕ_s with the currently available number of events, due to the very fast B_s^0 oscillation [18]. A production asymmetry, *i.e.* relative difference between the production cross sections of B_s^0 and $\overline{B}_s^0$ mesons, has an equivalent effect as a difference of mistag probability. Generator level studies estimate that the overall B_s^0 production asymmetry at LHCb is at the level of 1% [19], which causes a negligible bias in ϕ_s.

2.3 Decay time resolution

To account for the finite decay time resolution of the detector all time dependent functions in the PDF are convolved with a resolution model consisting of the sum of three Gaussians with a common mean. The parameters of the resolution model are determined from a fit that includes the prompt combinatorial background as discussed in [10]. The fit is shown in Figure 2 (left). The resolution parameters extracted from the fit are given in Table 3 where $\sigma_{1,2,3}$ is the RMS of each components, and f_2 (f_3) the fraction of the second (third) component.

[2] In the limit $\Delta\Gamma_s/\Gamma_s \to 0$ the relative uncertainty in the dilution translates into an equally sized relative uncertainty in $\sin\phi_s$.

σ_1 [fs]	σ_2 [fs]	σ_3 [fs]	f_2	f_3
33.7 ± 1.0	64.6 ± 1.9	184 ± 14	0.46 ± 0.04	0.017 ± 0.004

Table 3: Resolution parameters extracted from the fit explained in the text. The uncertainties are statistical only and highly correlated.

Just as for imperfections in the flavour tagging, the decay time resolution leads to a dilution of the oscillation amplitude [20]. For a mixing frequency of $17.8\,\mathrm{ps}^{-1}$, the effective dilution for our sample is given by

$$\langle \mathcal{D}^{\mathrm{reso}} \rangle_{\mathrm{eff}} \;=\; 0.68 \;\pm\; 0.04\,, \tag{13}$$

which corresponds to an effective decay time resolution of approximately 50 fs.

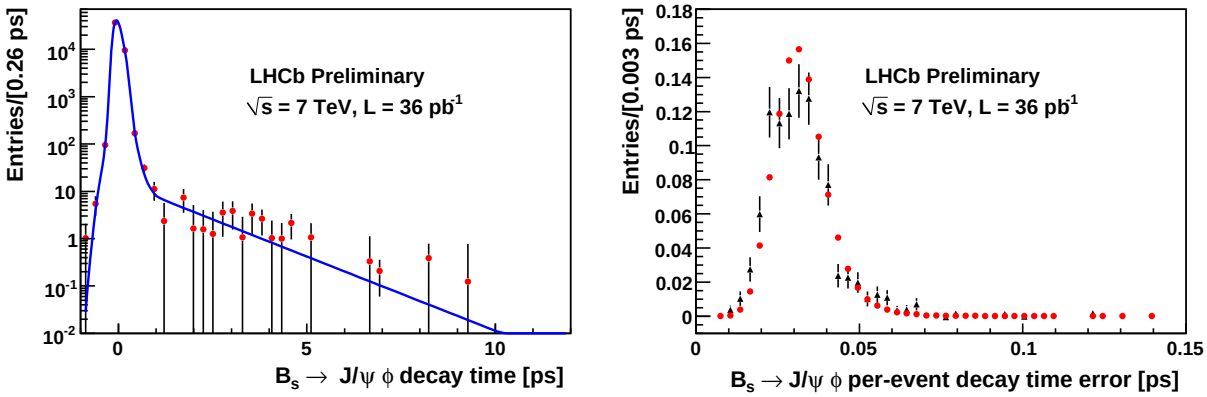

Figure 2: Left: Decay time distribution of background $B_s^0 \to J/\psi\phi$ candidates obtained with the sPlot [21] technique using the candidate mass as separating observable. The superimposed curve is the background decay time model convolved with the resolution model. The background model includes a prompt component and a long lived component, described by two exponential functions with different decay constants. Right: Distribution of the per-event decay time error for signal (triangles) and background (full, red circles) candidates, separated with the sPlot technique.

Uncertainties in the dilution arise from differences in the resolution between signal events and the prompt background events that are used to extract the parameters of the resolution model. We estimate this uncertainty by comparing the distribution of the per-event uncertainty on the measured decay time in data and using Monte Carlo simulations. Figure 2 (right) compares the distributions of per-event decay time uncertainty of signal and background candidate $B_s^0 \to J/\psi\phi$ events, in real data. The distributions, which have been statistically separated using the sPlot technique [21], do not exhibit a significant difference between signal and background. Using fully simulated events we find that the resolution obtained from prompt events is consistent with that for signal events within about 10%, leading to an uncertainty on the dilution of 6%.

2.4 Decay time acceptance

In addition to the resolution there are two lifetime acceptance effects. First, there is a shallow fall in acceptance for high lifetimes which affects both the "lifetime-unbiased" and the "lifetime-biased" datasets (the word "unbiased" therefore being a slight misnomer in this context). Second, there is strong drop for small lifetimes affecting the lifetime-biased dataset only. These acceptance effects are parameterized and accounted for in the maximum likelihood fit. The former is obtained from simulated events [10]. The latter is extracted from the data by using the overlap between the lifetimes-biased triggers and the lifetime-unbiased triggers. Figure 3 shows the fraction of lifetime-unbiased triggered events that have passed the biased trigger as well, as a function of the lifetime. The result of a fit with an empirical parameterization is used for the acceptance of the lifetime-biased events in the likelihood fit.

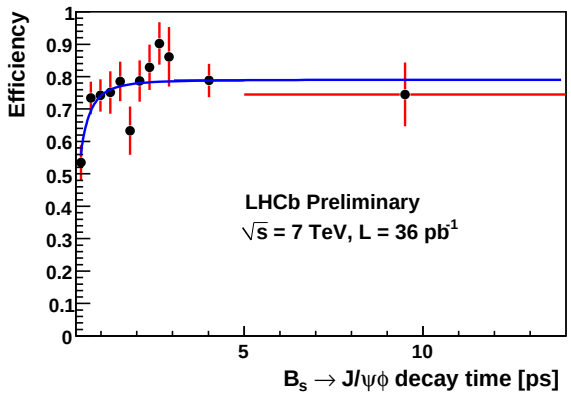

Figure 3: The histogram represents the efficiency of the biased trigger relative to the unbiased trigger, in real data. Superimposed is the result of the unbinned maximum likelihood fit to the model $\epsilon(t;a,c,n) \;=\; n\,(at)^c\,/\,[1+(at)^c]$.

2.5 Decay angle resolution and acceptance

The effect of the angular resolution on the decay angle distributions has been shown to be small [8] and is ignored in the signal modeling. Angular acceptance corrections are obtained from Monte Carlo simulations and taken into account in the likelihood fit [11]. Uncertainties on the corrections are derived from differences between data and simulation and lead to a bias on ϕ_s of at most a few percents [8].

3 Results

The 2010 data set does not constitute a sufficiently large sample of tagged signal events to constrain ϕ_s with a meaningful parabolic $\pm 1\sigma$ error. Therefore, we present the result of this analysis as two-dimensional confidence level regions in the $\phi_s - \Delta\Gamma_s$ plane obtained

using a likelihood ratio ordering, following the prescription of Feldman-Cousins (FC) [22]. By construction the FC confidence level contours provide the correct coverage for the physics parameters of interest. In addition, we provide a 68% CL for the projection of ϕ_s.

In order to quantify the effect of systematic uncertainties on the $\phi_s - \Delta\Gamma_s$ confidence contours, log likelihood contour scans[3] for systematically different fitting conditions have been performed and are compared to the confidence contours obtained with the nominal fit conditions. We find that all studied systematic variations of the fitting conditions have an insignificant effect on the $\phi_s - \Delta\Gamma_s$ confidence contours. The dominant systematic uncertainties are due to relative uncertainty in the dilution from flavour tagging (7%, Equation 12), the decay time resolution (6%, Equation 13) and ignoring a possible S-wave contribution (11%).

Figure 4 shows the projection of the fitted PDF on the combined lifetime-unbiased and lifetime-biased datasets for $t > 0.3\,\text{ps}$. Figure 5 shows the 68.3%, 90% and 95% FC confidence level contours in the $\phi_s - \Delta\Gamma_s$ plane. The contours exhibit a symmetry due to the two-fold ambiguity in relations 10. As stated above with our current $B_s^0 \to J/\psi\phi$ event yields we find systematic uncertainties have only a small effect on the contours. Therefore, the contours include only the statistical uncertainty, with the exception of the uncertainties due to flavour tagging calibration parameters and mixing frequency, which were floated in the fit. We find $\phi_s \in [-2.7, -0.5]\,\text{rad}$ at 68% CL and $\phi_s \in [-3.5,\ 0.2]\,\text{rad}$ at 95% CL when projecting the confidence level contours onto one dimension.

4 Conclusion

We have presented a tagged time-dependent angular analysis of $B_s^0 \to J/\psi\phi$ decays that allows us to constrain the CP-violating phase ϕ_s. Using $36\,\text{pb}^{-1}$ of pp collisions collected during the 2010 LHCb run at $\sqrt{s} = 7\,\text{TeV}$ we find 836 ± 60 $B_s^0 \to J/\psi\phi$ events. The average decay time resolution is 50 fs and the effective tagging efficiency, using only opposite-side taggers is $\epsilon\mathcal{D}^2 = (2.2 \pm 0.4)\%$. We reported the two-dimensional $\phi_s - \Delta\Gamma_s$ confidence region in Figure 5. The probability of a fluctuation from the Standard Model expectation to the observed result (i.e. the frequentist p-value) is 22%. Projected onto one dimension we find $\phi_s \in [-2.7, -0.5]\,\text{rad}$ at 68% CL.

[3] These are an order of magnitude faster to compute than the corresponding FC scan.

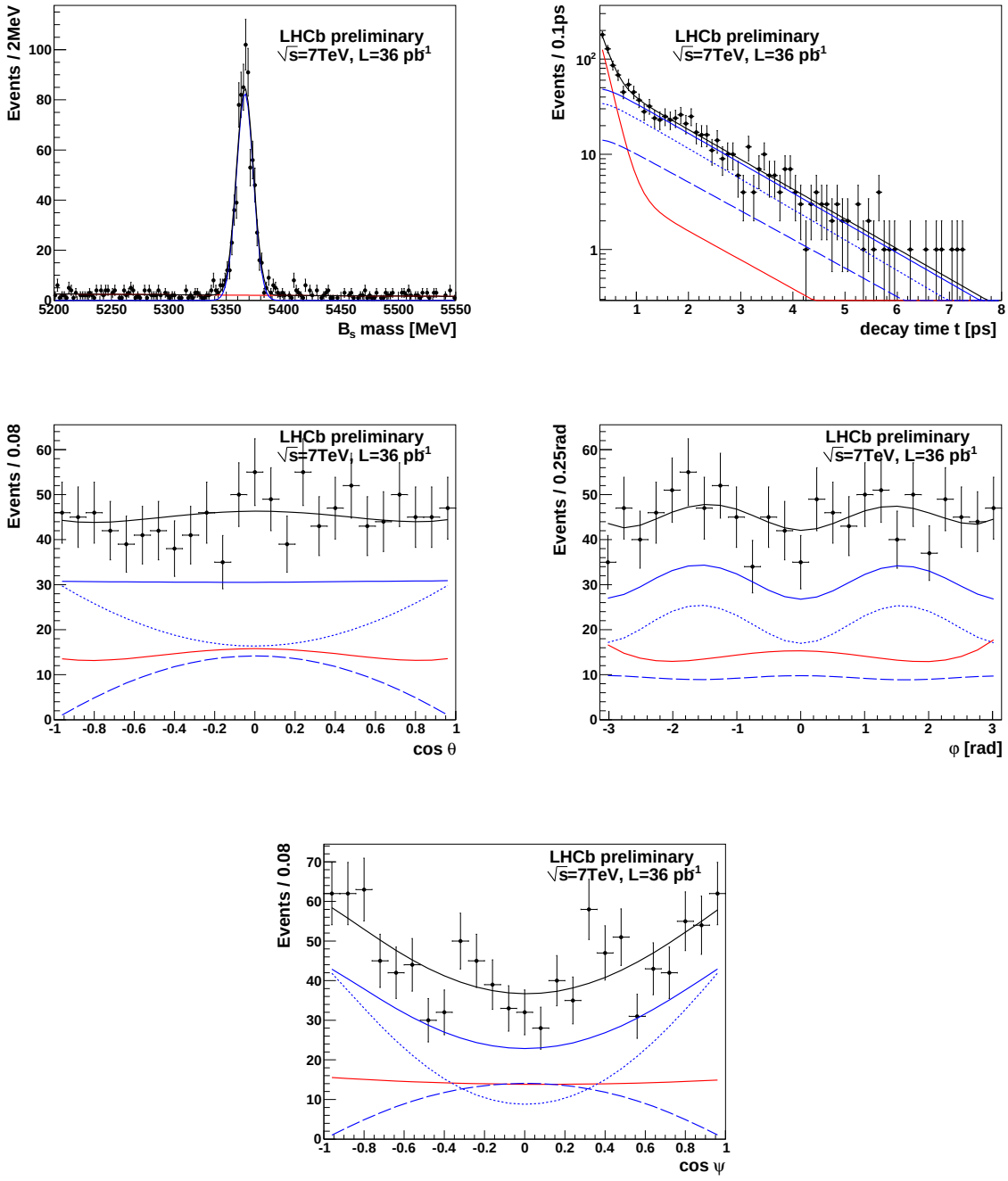

Figure 4: Projections for the biased and unbiased data sample after the tagged fit assuming $\phi_s = 0$. The decay time acceptances applied to the signal component are analogously applied to the background decay time distributions. The total fit result is represented by the black line. The signal component is represented by the solid blue line; the dashed and dotted blue lines show the CP-odd and CP-even signal components respectively. The background component is given by the red line.

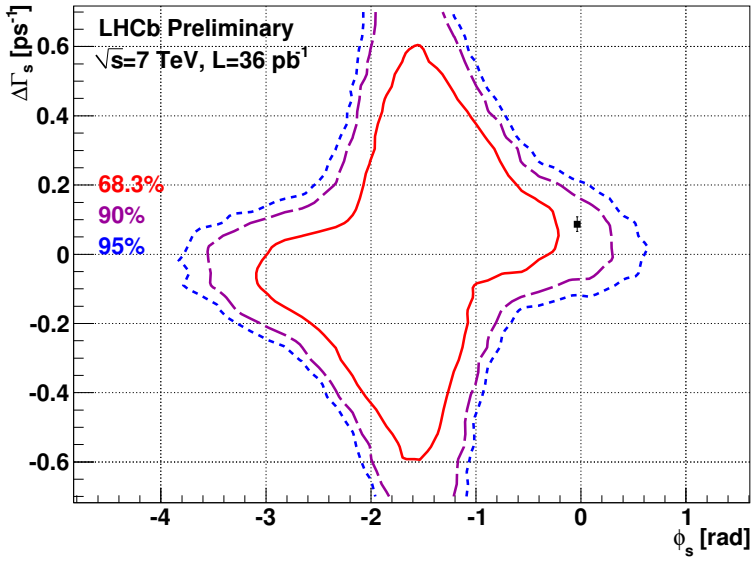

Figure 5: Feldman-Cousins confidence regions in the $\phi_s - \Delta\Gamma_s$ plane. The CL at the Standard Model point (black square) is 0.785 which corresponds to a deviation of "1.2σ". Projected in one dimension, we find $\phi_s \in [-2.7, -0.5]$ rad at 68% CL.

References

[1] J. Charles *et al.* (CKMfitter group), Eur. Phys. J. C41, 1-131 (2005), hep-ph/0406184, updated results and plots available at http://ckmfitter.in2p3.fr/

[2] A. Lenz and U. Nierste, "Theoretical update of $B_s - \bar{B}_s$ mixing," JHEP 0706 (2007) 072.

[3] A. Lenz and U. Nierste, "Numerical updates of lifetimes and mixing parameters of B mesons," arXiv:1102.4274 [hep-ph].

[4] Z. Ligeti, M. Papucci and G. Perez, "Implications of the measurement of the B_s^0–$\overline{B}_s^0$ mass difference", Phys. Rev. Lett. 97, 101801 (2006).

[5] See for example:
U. Nierste, "Bounds on new physics from B_s^0 mixing", Int. J. Mod. Phys. 22, 5986 (2008);
A. Lenz, "Unparticle physics effects in B_s^0 mixing", Phys. Rev. D 76, 065006 (2007);
R. Fleischer, "CP Violation and B Physics at the LHC".

[6] The CDF Collaboration, public note CDF/ANAL/BOTTOM/PUBLIC/10206 (2010).

[7] The D0 Collaboration, D0 Conference note 6098-CONF (2010).

[8] The LHCb Collaboration,"Roadmap for selected key measurements of LHCb.", LHCB-PUB-2009-029, arXiv:0912.4179.

[9] A. A. Alves *et al.* [LHCb Collaboration], "The LHCb Detector at the LHC," JINST 3 (2008) S08005.

[10] The LHCb Collaboration, "b-hadron lifetime measurements with exclusive $B \to J/\psi X$ decays reconstructed in the 2010 data", LHCb-CONF-2011-001.

[11] The LHCb Collaboration, "Untagged angular analysis of $B_s^0 \to J/\psi\phi$ and $B^0 \to J/\psi K^{*0}$ with the 2010 data", LHCb-CONF-2011-002.

[12] The LHCb Collaboration, "Optimization and Calibration of the Tagging performances using 2010 data", LHCb-CONF-2011-003.

[13] The LHCb Collaboration, "Measurement of CP violation in the time-dependent analysis of $B^0 \to J/\psi K_S^0$ decays with the 2010 data", LHCb-CONF-2011-004.

[14] The LHCb Collaboration, "Measurement of ΔM_s and calibration and tuning of the Same-Side Tagging algorithm with $B_s^0 \to D_s\pi$ decays using the 2010 data sample", LHCb-CONF-2011-005.

[15] The LHCb Collaboration, "Measurement of ΔM_d in $B^0 \to D\pi$", LHCb-CONF-2011-010.

[16] Y. Xie *et al.*, JHEP 0909:074, (2009).

[17] The CDF collaboration, "Observation of $B_s - \bar{B}_s$ Oscillation", Phys. Rev. Lett. 97, 242003, (2006).

[18] N. Styles *et al.*, "Measuring the weak phase in the decay $B_s^0 \to \phi\phi$ at the LHCb experiment", LHCB-PUB-2009-025.

[19] R. Lambert, "LHCb Hybrid Photon Detectors and Sensitivity to Flavour Specific Asymmetry in Neutral B-Meson Mixing" CERN-THESIS-2009-001.

[20] H. G. Moser and A. Roussarie, "Mathematical methods for B0 anti-B0 oscillation analyses," Nucl. Instrum. Meth. A **384** (1997) 491.

[21] M. Pivk and F. Le Diberder, "sPlot: a statistical tool to unfold data distributions", NIM A555 (2005) 356-369.

[22] G. J. Feldman and R. D. Cousins, "A Unified Approach to the Classical Statistical Analysis of Small Signals," Phys. Rev. D 57, 3873 (1998).